Wear 540-541 (2024) 205273

Contents lists available at ScienceDirect

Wear

journal homepage: www.elsevier.com/locate/wear

Recovery of metal matrix composite drilling tools using a WC-Ni/Cr TIG-hardfacing technology

Malek Hebib [a,b], Lilia Choukrane [a], Billel Cheniti [b,d,*], Lotfi Faghi [c], Alexandra Kovalčíková [d], Hamida Bouchafaa [c], Bouzid Maamache [b], Tamás Csanádi [d,e], Pavol Hvizdoš [d]

[a] Laboratory of Materials Technology (LTM), USTHB, BP 32 El Alia, 16111, Bab Ezzouar, Algeria
[b] Research Center in Industrial Technologies (CRTI), P.O.Box 64, Chéraga, Algeria
[c] Science and Engineering Materials Laboratory (LSGM), USTHB, BP 32 El Alia, 16111, Bab Ezzouar, Algiers, Algeria
[d] Institute of Materials Research, Slovak Academy of Sciences, Watsonova 47, 040 01, Košice, Slovak Republic
[e] Donát Bánki Faculty of Mechanical and Safety Engineering, Óbuda University, Népszínház utca 8, 1081, Budapest, Hungary

ARTICLE INFO

Keywords:
Metal matrix composite
As-infiltrated
TIG hard-faced coating
Interface
Wear loss

ABSTRACT

The recovery of worn and damaged drilling tools in oil and petroleum industries, which no longer meet reliable technological use, could significantly reduce the drilling cost and, therefore, the emission of toxic materials. The present study demonstrates first time an innovative solution for this problem using a WC-Ni/Cr Tungsten Inert Gas (TIG) hardfacing technology by which a damaged WC-based metal matrix composite was coated. The microstructure analysis of the recovered sample revealed remarkable diffusion activity of Cr and Cu elements across composite/hardfacing interface. This inter-diffusion depleted WC particles on both sides which enhanced the metallic bonding of the interface, creating a durable and strong adhesion. A significant amount of WC particles was fragmented and dissolved into the NiCr metallic matrix, which resulted in the formation of $Cr_{23}C_6$, W_2C carbides and Ni_2W_4C secondary carbide. There was found a more than 100 % increase in micro-hardness of the metallic matrix of the recovered sample compared to the as-infiltrated sample. The tribological tests of the as-infiltrated and the TIG hard-faced specimens conducted in dry, water and fuel oil environments revealed that the highest coefficient of friction (0.75) was recorded for the as-infiltrated sample under dry conditions with the highest wear loss (0.8 mg) while the TIG hard-faced coated one exhibited improved wear properties (0.09 and 0.15 mg, respectively). This was attributed to the change of wear mechanism from WC particle pullout to abrasive and oxidative wear through the formation of SiO_2 and WO_3 oxides films. Thus, the TIG hardfacing process shows new and promising technology to recover WC-based metal matrix composites, improving their lifetime, and at the same time, both their mechanical and tribological properties.

1. Introduction

In the petroleum industry, two types of drilling tools are usually employed, depending on their manufacturing process, namely matrix tool body and steel tool body. The first one was elaborated by powder metallurgy using the Sintering by Infiltration of Loose Powder (SILP) technique where a mixture of WC-based metal matrix composite (MMC) was infiltrated by transition elements such as Fe, Ni with Cu–Sn bronze binder. The second type was a steel body drilling tool obtained by hardfacing a tungsten carbide composite (e.g. WC-NiCr) on a machined steel [1,2]. These MMCs offer a unique combination of physical and mechanical properties (high hardness and strength, erosion and wear resistance and low thermal expansion coefficient, especially at high temperatures) that attracted much interest in tool industries and surface engineering and widened their application scope [3,4]. MMCs have been studied in detail by various researchers devising different methods to manufacture WC-based composite. Nevertheless, liquid phase sintering (LPS) remains the most popular and effective technique of their manufacturing. Conventional infiltration is type of LPS where the powder mixture was pressed into the desired shape then sintered at the molten temperature of the binder. In contrast to the conventional method of compressed and infiltration powder, non-conventional infiltration (SILP) allowed the production of tools (MMCs based material) with complex geometries, which cannot be manufactured by

* Corresponding author. Research Center in Industrial Technologies (CRTI), P.O. Box 64, Chéraga, Algeria.
E-mail address: ch.billel@gmail.com (B. Cheniti).

https://doi.org/10.1016/j.wear.2024.205273
Received 9 April 2023; Received in revised form 8 January 2024; Accepted 22 January 2024
Available online 26 January 2024

Table 1
Chemical composition of the materials.

Elements (Wt. %)	W	C	Ni	Cr	Fe	Cu	Sn	Mn	Mo
Powder mixture	58.4	35.6	6	-	-	-	-	-	-
hardfacing	61.42	9.84	22.52	4.89	1.33	–	–	–	–
Binder	-	-	10	–	0.5	78	6	5	0.5

conventional LPS techniques [5]. The efficiency of the MMCs using SILP, depends on the quality of the WC particles/matrix interface and the nature of the transition metal used as a matrix. Miroud et al. [6] suggested, for double-layer WC-15 %/and 14 %Ni composite elaborated by SILP, that the control of the working parameters (temperature of consolidation at 1180 °C and infiltration time) enhanced the homogeneity of particle distribution and avoided the interfacial precipitation. Tata et al. [7] investigated the infiltration of WC-W-Ni by a Cu–Mn alloy binder under different sintering conditions. They optimized the infiltration parameters at 30 min and 950 °C under a hydrogen atmosphere where Ni increased the densification and hardness of the binder phases. Similar results were obtained by Bouchafaa et al. [5] where the performance of the WC-W-Ni composite was significantly increased by adding Ni due to the formation of (Fe–Ni) solid solution and $FeNi_3$ at the particle/matrix interface, with high hardness and Young's moduli that were close to WC particles. Besides, Bouzagzi et al. [8] showed that the MMC configuration was strongly dependent on the components of the powder, especially the WC/W_2C amount and their interactions with the bronze binder. The inter-diffusion phenomena that occurred at the MMC/braze (Ag–Cu–Zn alloy) interface led to the formation of new phases of Cu–Zn, Ag–Zn, and the AgMn19 intermetallic compound, which was in good agreement with Cheniti el al [9]. Deshpande et al. [10] demonstrated that the good compatibility between WC particles and Cu-alloys and the excellent wetting features of Cu on WC particles enhanced the interfacial bond between the matrix and tungsten carbide particles. This was confirmed by Kennedy et al. [11] who studied whether spontaneous infiltration of ceramics by copper could occur and the effect of oxides and their geometry on wetting characteristics. The microstructural evolution of copper alloy matrix composites reinforced with WC particles and different Ni contents was extensively studied by Daoud et al. [12]. The increased Ni content above 3 % promoted the decrease of the microstructural features and composites properties with the enhancement of the wettability between the molten metallic matrix and the reinforcement particles.

WC-based coatings are the most common cemented carbides used today that combine the hard WC particles with the ductile metallic matrix. These MMCs operate under severe conditions of high temperatures and withstand a wide range of loads without altering their good mechanical and tribological properties. Many studies have been published on the effect of the metallic binder nature on the mechanical and the tribological behavior of thermally sprayed WC-based coatings [13–16]. Cobalt is the most widely used binder due to its good wetting of WC particles whereas, because of their low cost and better corrosion resistance, Ni and Cr–Ni have also been employed as binders despite their weak metallurgical and mechanical benefits over Co [17]. Nickel-based alloys have for a long time been used as a metallic matrix using different coating deposition techniques. Tobar et al. [18] deposited WC-reinforced composites based on a self-fluxing NiCrBSi alloy powder by laser cladding. The porosity level, micro-hardness and particle distribution were affected by the proportion of WC particles in the metallic alloy. Maazouzi et al. [19] studied structure evolution, tribological and mechanical properties of heat treated HVOF NiCr–WC10Co MMCs where the NiCr–Co metallic matrix was selected because of its excellent adhesion to the steel substrate, superior corrosion resistance and compatibility with WC particles. Wang et al. [20] deposited WC with a NiCr-based matrix by laser cladding on carbon steel. They found diffusion-controlled shells around the WC particles. In another study, TIG welding was adopted to deposit Ni-WC powder on AISI 1010 steel. The microstructure, mechanical and wear behavior of the cladding were strongly influenced by the TIG parameters (heat input, current, speed, gas flow etc.) [21]. Boytoz et al. [22] found that the higher the heat inputs gave greater WC particle dissolution, which affected the hardness and the tribological behavior of the WC TIG claddings. Similar results were found by Singh et al. [23] who established that at low heat input,

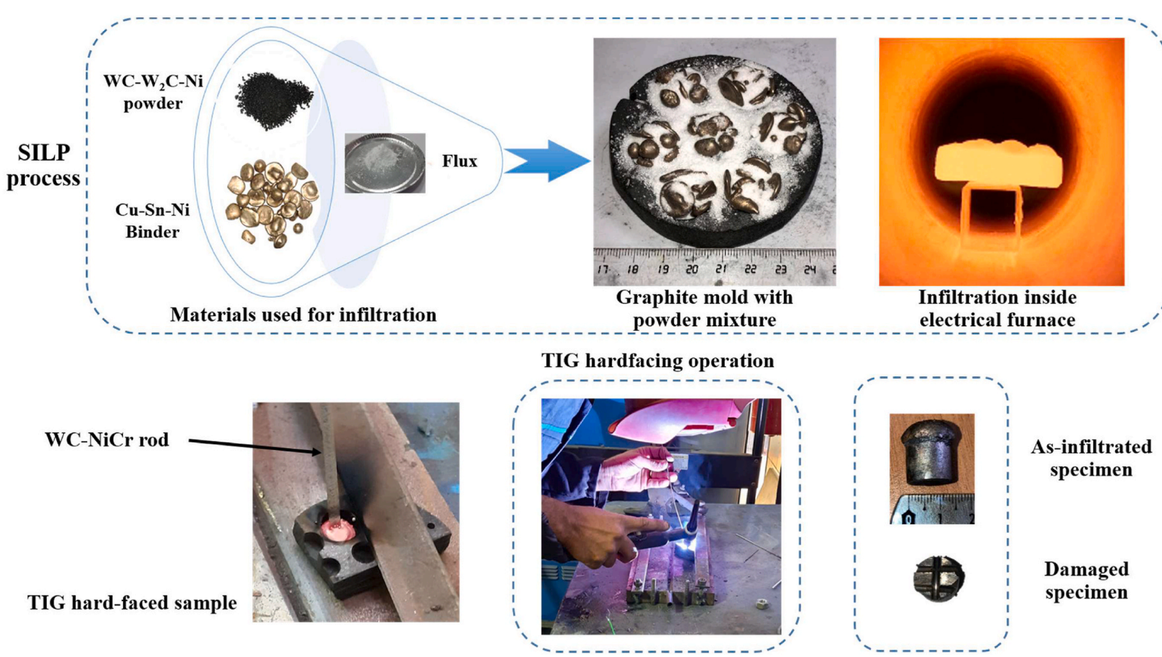

Fig. 1. The experimental processes for powder sintering by infiltration and TIG hardfacing technique.

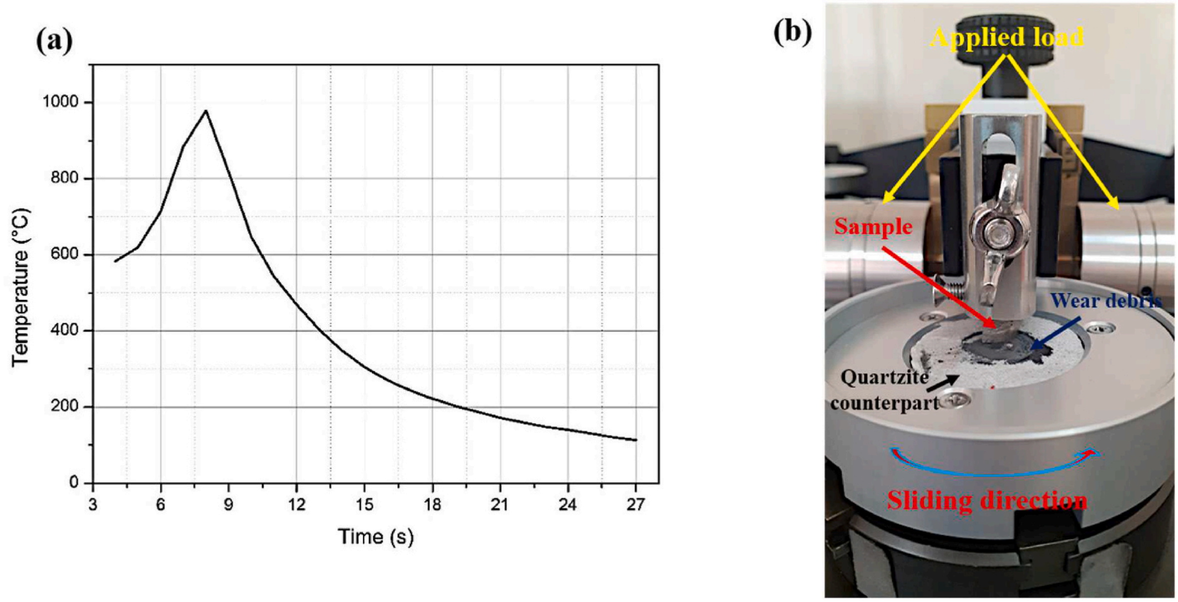

Fig. 2. (a): Thermal cycle recorded during hardfacing operation, (b): Sample emplacement during wear tests.

the WC-Co-Cr cladding obtained by TIG process, exhibited a high hardness and wear resistance due to the partially molten WC grains in Co–Cr matrix.

Regardless of the type of drilling tools (matrix or steel body) used in petroleum or other industries, after they're worn out, those are needed to be replaced which is costly since they consist of critical raw materials (W, Co) and are toxic to the environment (Co). The recovery of worn and damaged drilling tools would be a cost-saving and environment-friendly solution for this problem. However, to the authors' best knowledge, no study has been conducted to recover and reuse WC-based matrix-body drilling tools after their service life so far. Therefore, the present work aims to demonstrate first time an innovative solution for this problem by recovering a metallic matrix drilling body (WC-based composite) obtained by SILP process using TIG hardfacing technique. To shed light on the promising recovery process, the interaction between WC particles and metallic matrix was explored. Additionally, the effect of the TIG process on the integrity of WC particles and their decarburization was also studied. To verify the enhanced physical performance of the recovered drill tool, microstructural, mechanical and tribological investigations were done systematically both on the MMC and TIG hard-faced samples that have been subjected to wear tests in dry and wet (water and fuel oil) environments.

2. Material and methods

The powder used to fabricate the MMC consolidates was provided by the Algerian company of well services (Entreprise Nationale des Services au Puits, ENSP. Sonatrach). A mixture of raw powders of WC/W_2C–5W–5Ni with 90 wt% bi-phasic tungsten carbide (WC/W_2C), 5 wt % W and 6 wt% Ni particles were blended for 2 h to infiltrate the system by a Cu–Sn-based binder. Table 1 shows the chemical composition of the base materials obtained using optical emission spectrometer analysis Oxford Foundry Master Pro. The infiltration of powder mixtures was conducted inside a graphite mold using an electrical furnace as illustrated in Fig. 1. The sintering temperature was fixed at 1180 °C based on the differential thermal analysis results of the Cu–Sn binder. The melting point of the Cu–Sn binder was 1030 °C to which was added 150 °C to ensure and maintain the alloy in a liquid state during the sintering period. The system was held for 30 min at this temperature and cooled in the furnace. The surplus of the binder (residual quantity) remained at the higher part of the composites after infiltration was cut and the samples were mechanically polished and cleaned. Thereafter, one composite was damaged by surface machining while the second one remained undamaged as shown in Fig. 1. Tungsten Inert Gas (TIG) welding process was used as hardfacing technique to deposit WC-NiCr rod on the damaged specimens (Fig. 1) adopting a direct current negative electrode (DCEN) mode with 150A, 20V voltage under argon shielding gas (10 l/min flow rate). The main compositions of the WC-NiCr rod used in this study was given in Table 1.

Table 2
Wear test parameters.

Applied load (N)	10
Counterpart	Quartzite stone
Sample cross-section area (cm^2) As infiltrated	0.5
Sample cross-section area (cm^2) TIG hardfacing	0.3
Sliding time (h)	18.5
Sliding distance (m)	2000
Wear track diameter (mm)	5
Velocity (mm/s)	30
Temperature (°C)	26
Humidity	60 %

The thermal cycle (Fig. 2a) during the hardfacing operation was checked and recorded using a 0.5 mm diameter K-type (alumel-chromel) thermocouple inserted 3 mm from the top surface of the damaged samples by wire electrical discharge machining. Before characterization, the samples were cut longitudinally to the infiltration and hardfacing direction and prepared for metallographic analysis using standard techniques of grinding and mechanical polishing. Microstructural examination of samples was done using a Nikon ECLIPSE LV100D-U optical microscope and a Zeiss EVO scanning electron microscope. An energy dispersive X-ray spectrometry (EDS) microprobe was used to identify the chemical compositions at different regions of the composites and the hard-faced samples. Hardness (HV30) and micro-hardness (HV0.3) measurements were (four indents for each load) along the cross-sectional from the as-infiltrated composite towards the TIG hard-faced surface using a INNOVEST-9000 with 30kg/f and a Buhler with 0.3kgf. XRD was performed using a Discovery D8 Bruker diffractometer, with 40 kV, Co Kα radiation = 0. 1.7896 nm and 0.05°/s step size. The recorded XRD patterns were characterized by High Score software using PDF4 database. This technique was used to characterize the as-

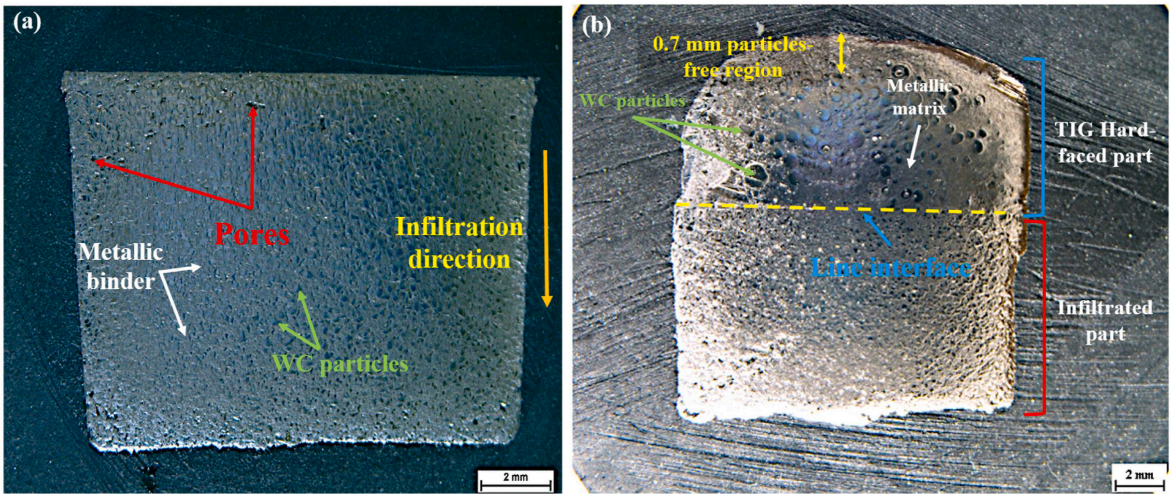

Fig. 3. Macrographic images of (a): as-infiltrated specimen and (b): TIG hard-faced specimen.

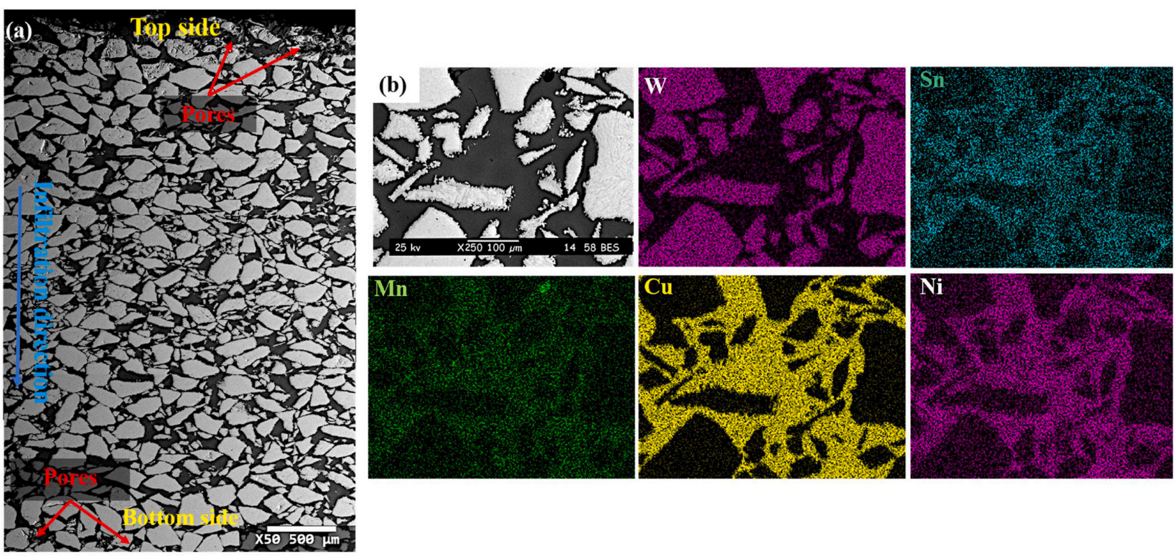

Fig. 4. As-infiltrated sample (a): SEM-BSE micrograph of the cross section showing top and bottom surfaces, (b): EDS maps of elements distribution in the as-infiltrated specimen.

infiltrated and TIG hard-faced samples before and after wear tests.

Pin-on-disc tribological tests were conducted on a CSM tribometer (CSM Instruments Inc, Peseux, Switzerland) with the experimental conditions summarized in Table 2. The tested samples were polished to have the same surface finish and placed as the pin (Fig. 2b) while the counterpart was quartzite stone which is hard to perforate during well drilling operations in the Algerian Sahara. The first series of tests were carried out in dry conditions without lubrication to assess the resistance of the samples under extreme operating conditions (lack and/or interruption of lubricant). The second series of tests were performed with two different lubricants, water and fuel oil (Gasoil with 0.835 kg/m^3 density at 15 °C and 0.25 wt% of Sulphur) conditions. The choice of these solutions was related to the lubricant used during plugging and drilling operations to evaluate the effect of lubrication on the friction properties of the sample surfaces. All tests were repeated five times at room temperature and the friction coefficient was continuously measured and recorded in real-time by TriboX. At the end of each test, the wear loss of samples and quartzite stones was measured and the wear tracks were analyzed by SEM-EDS. The specimen observations of the worn surfaces were performed by atomic force microscopy (AFM) using a ScanAsyst, (Bruker instrument) in PeackForce tapping mode. All the images were recorded and processed using Nanoscope V software (Veeco) to measure the surface roughness.

3. Results and discussion

3.1. Microstructural evolution of the consolidated and the TIG hardfaced samples

Fig. 3 shows the macrographs cross-section of the as-infiltrated and TIG hardfaced specimens. The WC particles were homogeneously distributed throughout the as-infiltrated sample and no segregation of WC particles was observed in the bottom and top sides with some pores detected throughout the composite (Fig. 3a). The thickness of the TIG hard-faced coating was approximately 6 mm whereas the hardfacing/composite interface was less clear in Fig. 3b. The spherical WC particles with 0.2–1 mm size were clearly observed in the TIG hard-faced coating whereas the as-infiltrated specimen exhibited irregular WC particles with smaller size. The top side of the hard-faced sample had a particles-free region of 0.7 mm thick as a result of the gravity force that pulled the

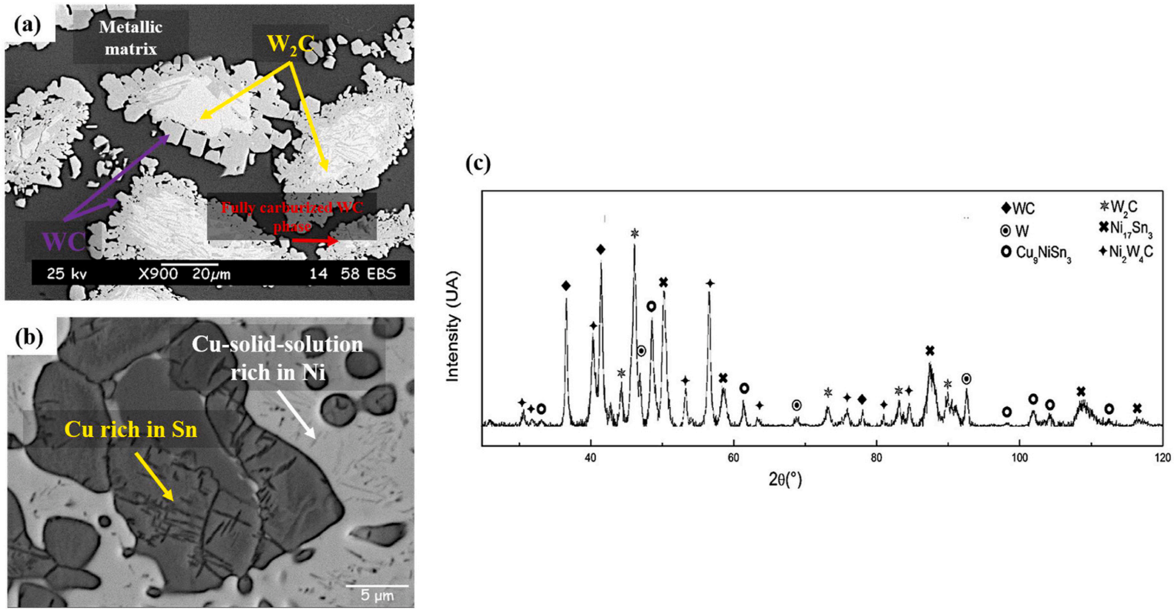

Fig. 5. As-infiltrated specimen, (a): SEM-BSE micrograph of the MMC, (b): SEM-BSE micrograph of the metallic binder and (c): XRD pattern conducted in the middle part of the sample.

WC particles down due to their high weight during the TIG hardfacing operation.

Fig. 4a shows SEM cross-section micrograph of the as-infiltrated composite. A weak porosity level was detected in the entire composite, which reflected that the infiltration process occurred under sufficient capillary forces to guarantee the densification of the composite. Besides, WC/W_2C particles showed irregular sizes ranging between 50 and 200 μm that are homogenously distributed with no de-bonding or crack defects detected at the particles/binder interface. This indicated the complete dissolution of Ni into the metallic matrix (Fig. 4b), which enhanced the capillarity forces and wettability of the WC particles by the molten binder and consequently increased the densification of the composite [24]. These results were in good agreement with Daoud et al. [12] who related this behavior to the strong interfacial bond and the excellent wetting characteristic of WC and Cu elements [25].

Furthermore, the lack of evidence of chemical interaction between WC and Cu, suggested that no intermetallic compounds were formed at the WC particles surface, which should have eased the sintering process [26]. Despite the high wettability observed in the micrographs at the top and middle regions of the as-infiltrated composite, some residual pores were detected at the top and bottom sides as shown in Fig. 4a.

Two different regions were identified in the as-infiltrated microstructure (Fig. 5a), which included white and dark phases. These were bright W_2C phases with needle shapes (Fig. 5a) surrounded by irregular grey WC phase within particles, the whole embedded in a dark metallic matrix. The simultaneous presence of WC and W_2C phases (Fig. 5a) suggested that the carburization phenomena of WC particles was interrupted during manufacturing process. This phenomenon was deeply investigated by Mühlbauer et al. [27] who demonstrated that during sintering, W_2C phase is transformed to WC phase by carburization reaction. Zhengji [28] revealed that when carbon is in direct contact with W surface, a fast initial formation of WC rim is occurred. The W presents in the core of the particle is converted to W_2C phase followed by a much slower reaction of W_2C into WC phase. It is clear on Fig. 5a that the carburization transformation of W_2C to WC is not finished. As shown in the right side in Fig. 5a, some particles showed a fully carburized WC phase while others exhibited continuous growth of WC phase with platelet shape.

The metallic matrix exhibited a fine dendritic structure with no preferential orientation as shown in Fig. 5b. The EDS point analysis revealed an important chemical heterogeneity into the inter-dendritic spacing with pronounced Sn and Ni content. Meanwhile, a high amount of Cu and Ni is detected in the dendritic phase (Fig. 5b), According to EDS mapping analysis shown in Fig. 4b and XRD spectrum (Fig. 5c), this phase corresponds more probably to Cu-solid-solution rich in Ni element. Besides WC, W_2C and Cu_9NiSn_3 phases (Fig. 5b), also the

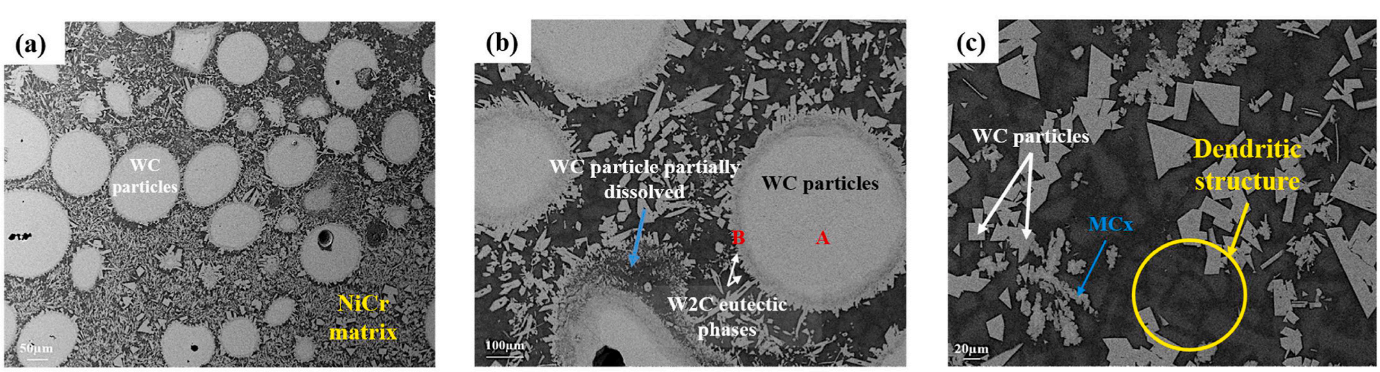

Fig. 6. Cross-section of TIG hard-faced coating (a): SEM-BSE micrograph of the hardfacing, (b): high magnification of the WC particle/NiCr matrix interface, (c): the metallic matrix.

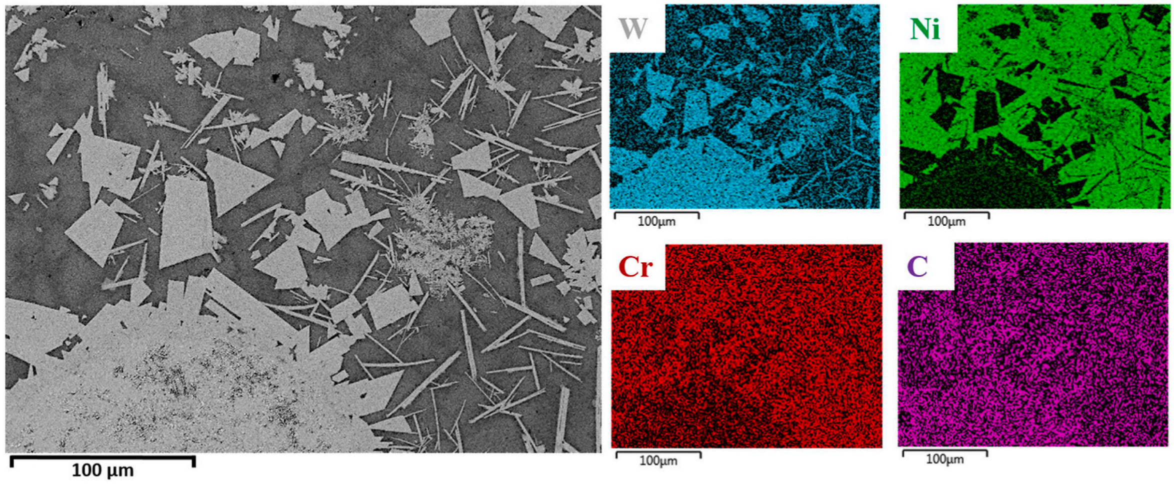

Fig. 7. SEM-BSE micrograph of the WC/NiCr interface of the TIG hard-faced coating with the EDS maps of elements.

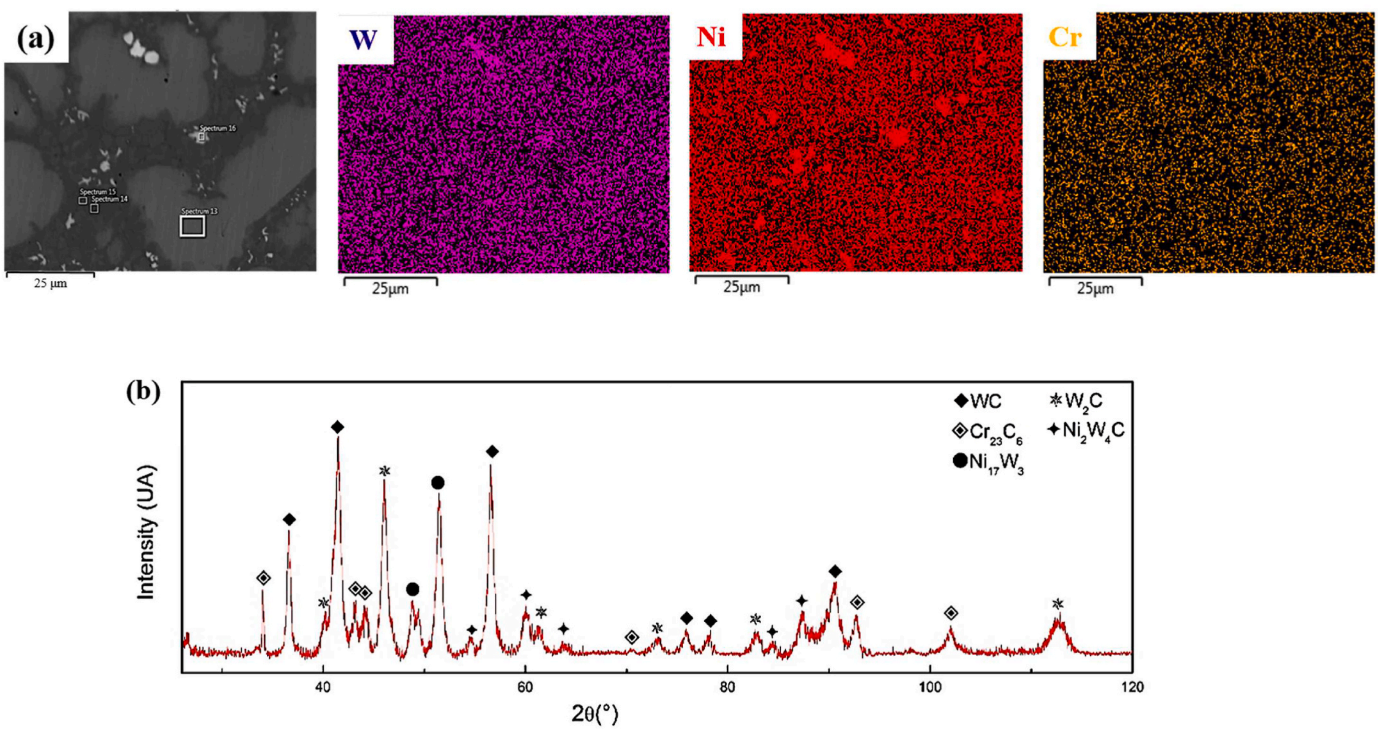

Fig. 8. TIG hard-faced coating (a): SEM-BSE micrograph of the hardfacing metallic matrix with its corresponding EDS maps analysis (b): XRD pattern of the TIG hard-faced coating.

secondary carbide Ni_2W_4C formed after the long infiltration time (30 min). This may indicate some decarburization of the composite as the WC particles dissolved due to the working temperature (1180 °C) reached during infiltration process.

Fig. 6a shows the SEM micrograph of the TIG hard-faced coating. Compared to recent research works on WC TIG cladding [29], the dissolution degree of WC particles into the metallic matrix was remarkably high. As shown in Fig. 6a, the dark metallic matrix is hardly distinguished due to the considerable amount of small bright particles uniformly distributed throughout the matrix. It is known that the fragmentation and dissolution of WC particles are thermally activated. In TIG hardfacing process, the increased applied current (150A) generates high thermal input causing a partial dissolution of WC particles (Fig. 6b) into the molten pool, which resulted in the formation of carbides during solidification (Fig. 6c). On the other side, the employment of low TIG current [30] or low energy generating hardfacing process (oxyacetylene and plasma) produced undamaged WC particles [2,31]. Besides, no agglomeration of WC particles occurred and they uniformly distribute throughout the hardfacing coating (Fig. 6a). Additionally, WC particles appeared with different shapes (Fig. 6b and c), where some particles are spherical surrounded by W_2C eutectic phase and there are additional small polygonal shape WC particles which probably transformed from the W_2C phase.

EDS mapping analysis of the WC particle/metallic matrix interface of the TIG hardfacing coating is shown in Fig. 7. The presence of W within the matrix constituent can be attributed to the pronounced dissolution of tungsten carbides (WC) within the molten nickel binder during TIG hardfacing operation. This dissolution, shown in Fig. 7, is initiated through an inter-diffusion mechanism, activated when the WC particles become encapsulated by the molten metallic binder. Throughout the

Table 3
EDS point analysis conducted on Figs. 6b and 8b.

Elements Wt. %	W	C	Ni	Cr	Cu	Sn
A	95	5	–	–	–	–
B	79	7	8	6	–	–
C	4	–	15	6	49	26
D	2	–	22	8	42	21
E	6	–	69	11	12	2

deposition process, this dissolution is further expedited due to the substantial chemical affinity between Ni, W, Cr and C [32]. The mutual diffusion of these chemical compounds significantly reinforces the bond between the WC carbides and the metallic matrix, thereby rendering the detachment of the carbides more difficult, which enhance the wear resistance of the coating. On the other side, Liu et al. [33] reported that the dissolved W and C that react with metallic matrix elements (Ni and Cr) may promotes the re-precipitation of new small-size carbides surrounding the WC particles that could impair the hardness properties of the coating.

EDS mapping analysis of the metallic matrix (spectrum 13 in Fig. 8a) disclosed that the main chemical component of some of these particles to be ~ 55 at.%W ~ 32 at.%Ni and ~ 13 at.%C, being qualitatively in good agreement with Ni_2W_4C secondary carbide stoichiometry.

Small particles started to dissolve by forming new particles in form of platelets as shown in Fig. 6c. It should be mentioned that the volume fraction of WC particles after TIG hardfacing operation, measured using image analysis, is about 60 %, which represents a reduction of 15 % compared to its initial content. This phenomenon is related to the WC particles' dissolution at high temperatures. In the TIG hardfacing operation, the metallic matrix melted first, followed by the fragmentation and the dissolution of both small WC particles and the surrounding WC big particles in the liquid matrix as a result of the chemical affinity between WC and Ni elements [32]. This dissolution caused important microstructural changes in the hardfacing coating (Fig. 6a), including the formation of undesirable intermetallic phases: $Cr_{23}C_6$, eutectic W_2C phase and Ni_2W_4C secondary carbide at the peripheries of the WC particles as shown by XRD spectrum in Fig. 8b. Furthermore, according to W–Ni binary phase diagram [32] W favored the solidification of dendritic phase (metallic matrix) at the first place during cooling due to the high melting point [2]. The EDS point analysis, conducted at the top region of the hardfacing (Table 3 targeted point in Fig. 6b), revealed a

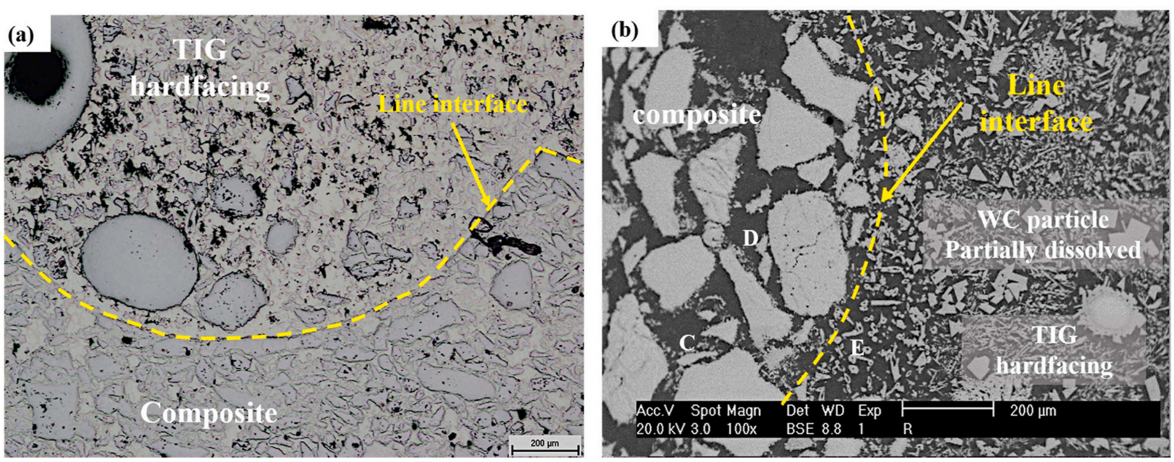

Fig. 9. Micrographs of composite/TIG hardfacing interface. (a): optical micrograph and (b): SEM-BSE micrograph.

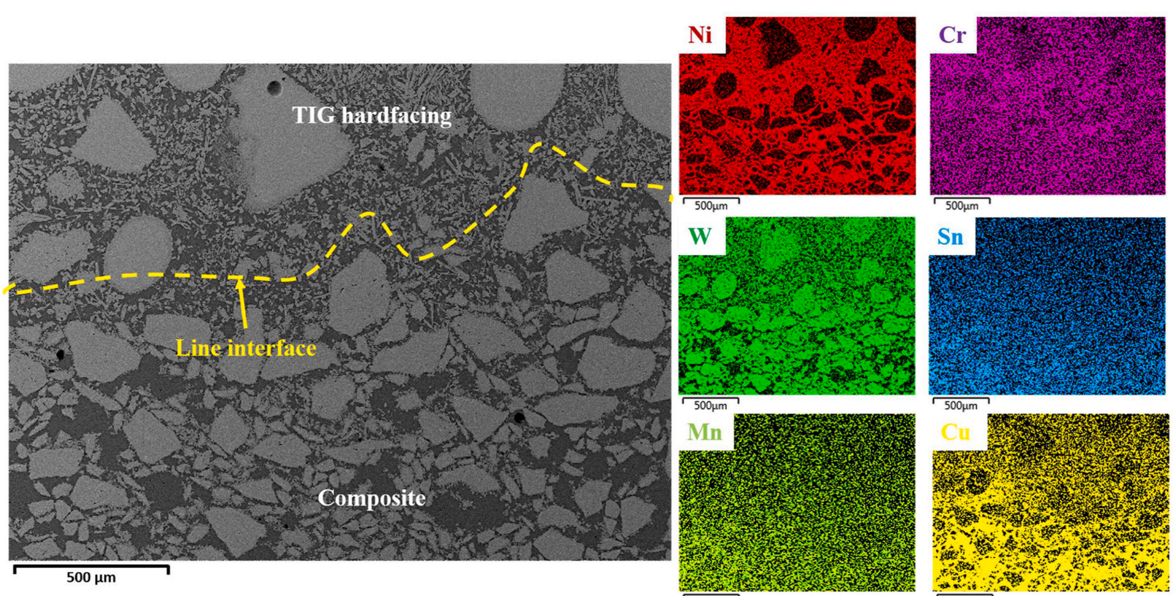

Fig. 10. SEM-BSE micrographs of composite/TIG hardfacing interface with EDS maps analysis.

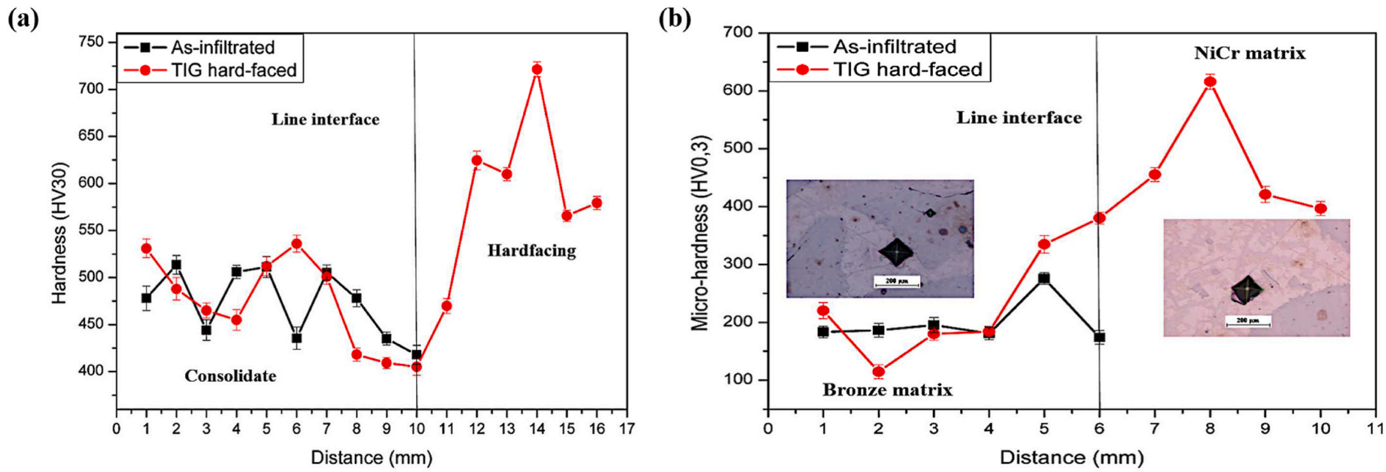

Fig. 11. Hardness evolution along the composite and the TIG hard-faced samples (a): Hardness HV30 and (b): Micro-hardness HV0,3 performed on the metallic matrix.

decrease in W concentration from the interior of WC particle (95 wt % in spot A) towards the NiCr matrix interface (79 wt % in spot B). This suggested the dissolution of WC particles into the matrix due to the solubility of W in Ni (~9 %), according to the W–Ni binary phase diagram [32]. The formation of the intermetallic phases in the soft metallic matrix, as a result of the decomposition and the dissolution of WC particles (Fig. 8a), may directly affect the mechanical properties of the coating, which influences its wear performances.

Fig. 9a is an optical micrograph of the cross-section of TIG hard-faced interface. The line interface was identified by the large irregular WC particles that seemed to act as a barrier stopping the insertion of small platelet WC particles from the coating. Fig. 9b shows high amounts of irregular WC particles were found in the hardfacing side with some large WC particles partially dissolved. The EDS point analysis, conducted in some regions around the interface (Table 3), revealed an important content of Cr element in the binder phase (Spot C and D in Fig. 9b) of the composite that diffused from the hardfacing coating. While the high concentration of Cu element (Spot E) is detected in the hardfacing coating due to the chemical affinity between Ni–Cu and Cr that is enhanced at a high working temperature [24]. This mutual distribution of elements across the WC-Ni TIG coating/composite interface is highlighted throughout the EDS mapping analysis shown in Fig. 10. It is evident that the W element, representing WC particles, is uniformly and homogeneously distributed throughout all the interface. where no areas devoid of W is observed. Additionally, high diffusion of Ni and Cr towards the composite accompanied with the diffusion of Cu and Sn towards the hardfacing coating are clearly visible. This results in high metallurgical bonding and strengthen the interface by boosting the diffusion activity throughout the composite/hardfacing interface, which may have enhanced the mechanical and tribological properties of the hardfacing.

3.2. Hardness and micro-hardness evolution

The hardness measurements between the composite and the TIG hard-facing specimens are illustrated in Fig. 11a. In the infiltrated part, both specimens exhibit roughly similar tendency, i.e., the hardness at the bottom was around 480 ± 15 HV30 and it decreased immediately to 420± 12 HV30 reaching the top side of the composites. This was caused by a more metallic binder which is ductile (Cu, Sn) that reduced the overall hardness of the top region of the composite. The hardness increased to its maximum value in the TIG-hardfacing coating and reached 650 ± 13 HV30. The presence of W_2C eutectic phase, chromium carbides with high concentration of fragmented WC particles in the metallic matrix are at the origin of the increase in hardness. Furthermore, a slight decrease in hardness is observed on the upper region of the TIG hardfacing coating near the extremity, which is attributed to the WC free-particles region already identified in Fig. 3b.

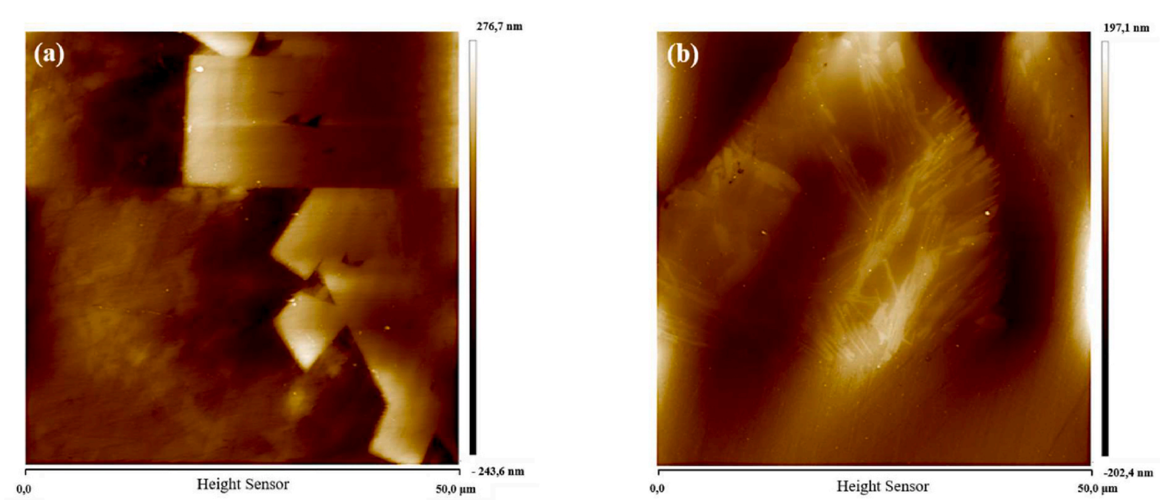

Fig. 12. 2D AFM topography of (a): TIG hard-faced sample surface and (b): as-infiltrated surface prior wear tests.

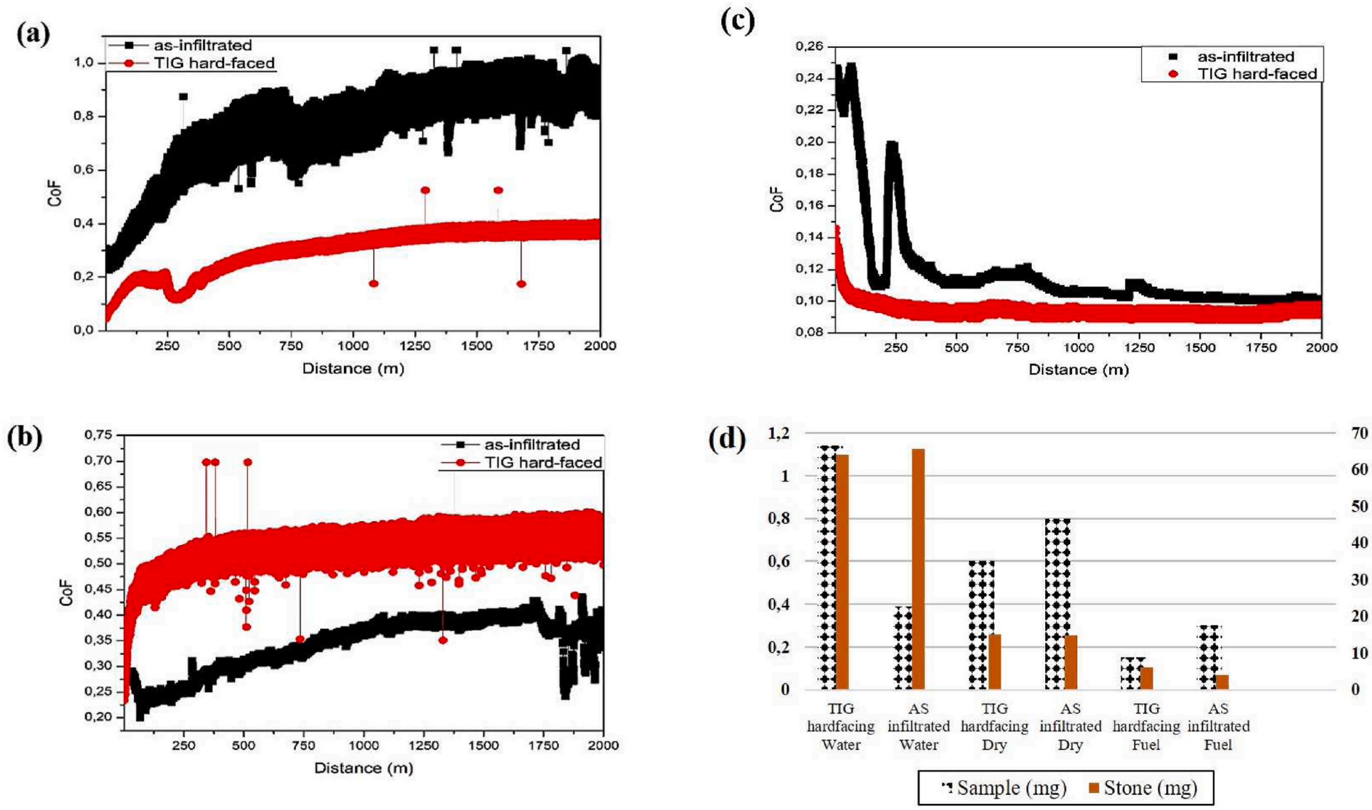

Fig. 13. Evolution of wear properties (a): CoF in dry condition, (b): CoF under water, (c): under fuel environment and (d): wear loss of samples under different conditions with their respective quartzite stone counterparts.

The micro-hardness measurements conducted on the metallic binder on both specimens (Fig. 11b) showed that, after hardfacing, the metallic matrix at the interface becomes harder (approximately twice as hard as at the as-infiltrated matrix). This can be explained by two main factors:

(i) : The concentration of a high amount of small platelet WC particles dissolved into the metallic matrix due to the high temperature (976 °C) reached during hardfacing operation (see the thermal cycle in Fig. 2a) as described in section 3.1.

(ii) : The diffusion of Ni and Cr elements from the hardfacing coating towards the interface line as a consequence of mutual chemical affinity with Cu of the composed matrix. These elements at this location caused a strong increase in hardness (480 ± 16 HV0.3) as reported by Lee et al. [34] and Uzkut et al. [35].

3.3. Tribological investigation

Prior the wear tests, both TIG hardfaced coating and composite samples were polished to achieve similar surface finish of Ra ~ 50 nm roughness as shown in Fig. 12a and b. The evolution of the coefficient of friction (CoF) with a sliding distance of as-infiltrated and TIG hard-faced samples tested in dry condition, in water and fuel environments are shown in Fig. 13a, c. The CoF under different conditions were similar for both samples. For the dry condition testing, both samples exhibited an increase in CoF during the initial run-in period (10–250 m), before reaching a steady-state value of 0.75 and 0.3 for as-infiltrated and TIG hard-faced samples, respectively. It is not necessarily true that there is an inverse relationship between hardness and CoF. Numerous research works [36–41] reported that statement. However, it is not an absolute rule and should be considered within the context of the specific materials and conditions of a given application. The relationship between hadrfacing coating hardness and COF can be more complex and depends on various factors, including the specific materials involved, their chemical compatibility, adhesion with the substrate, the coating surface state, lubrication, operating conditions and especially the dominant wear mechanisms [42,43]. In the present study, both WC-NiCr TIG coating and composite had similar surface roughness of approximately 50 nm to insure the same contact between the surfaces at the beginning of wear tests. On the other side, the strong chemical compatibility between the hardfacing coating and the composite is well highlighted through the mutual inter-diffusion of elements across the defect-free interface (see section 3.1). This reflects the good adhesion between the TIG coating and the composite which can lead to lower friction [44,45]. It is interesting to note that despite the remarkable difference in hardness between the TIG hadrfacing coating (600 HV30) and the composite (450 HV30), this cannot be the only factor that predict the CoF trend. As shown in Fig. 4a, the detected pores on the composite not only contribute to an increase in its CoF but also exert a notable influence on its wear mechanism.

Under wet sliding, numerous factors contribute to the wear process of materials such as water film, temperature of the fluid and its viscosity [46]. During water sliding (Fig. 13b), the samples exhibited different increasing CoF behavior upon reaching steady-state. The as-infiltrated sample showed a wider CoF shape slope where the steady state (0.34) was reached after a long run-in period (1100 m). The CoF value of the hard-faced sample was much higher (0.52) with fewer fluctuations where the steady state was reached after a short run-in period (200 m). The change in CoF behavior was more likely attributed to the change in the wear mechanisms of the composites with the existence of the lubricant. As expected, the lowest CoF values were obtained in the fuel environment (Fig. 13c) for both samples with a roughly similar value of 0.1. The reduction in CoF values, considering the different sliding conditions, reflects the effective lubrication role that plays the latter in both samples compared to dry conditions. Notably, less fluctuation in CoF values can be observed for fuel (Fig. 13c) compared to the water environment, as well as for the water environment when compared to dry

Table 4
CoF values with wear loss measurements issued from different wear conditions.

	CoF		Sample wear loss (mg)		Stone wear loss (mg)		Sample/stone wear ratio (x10^{-2})	
	As infiltrated	TIG hardfacing	As infiltrated	TIG hardfacing	As infiltrated	TIG hardfacing	As infiltrated	TIG hardfacing
Dry sliding	0.75	0.3	0.8	0.6	14.8	15.06	5.4	3.9
Water sliding	0.34	0.52	0.39	1.14	65.74	64.04	0.6	1.8
Fuel sliding	0.11	0.09	0.3	0.15	4.15	6.17	7.2	2.4

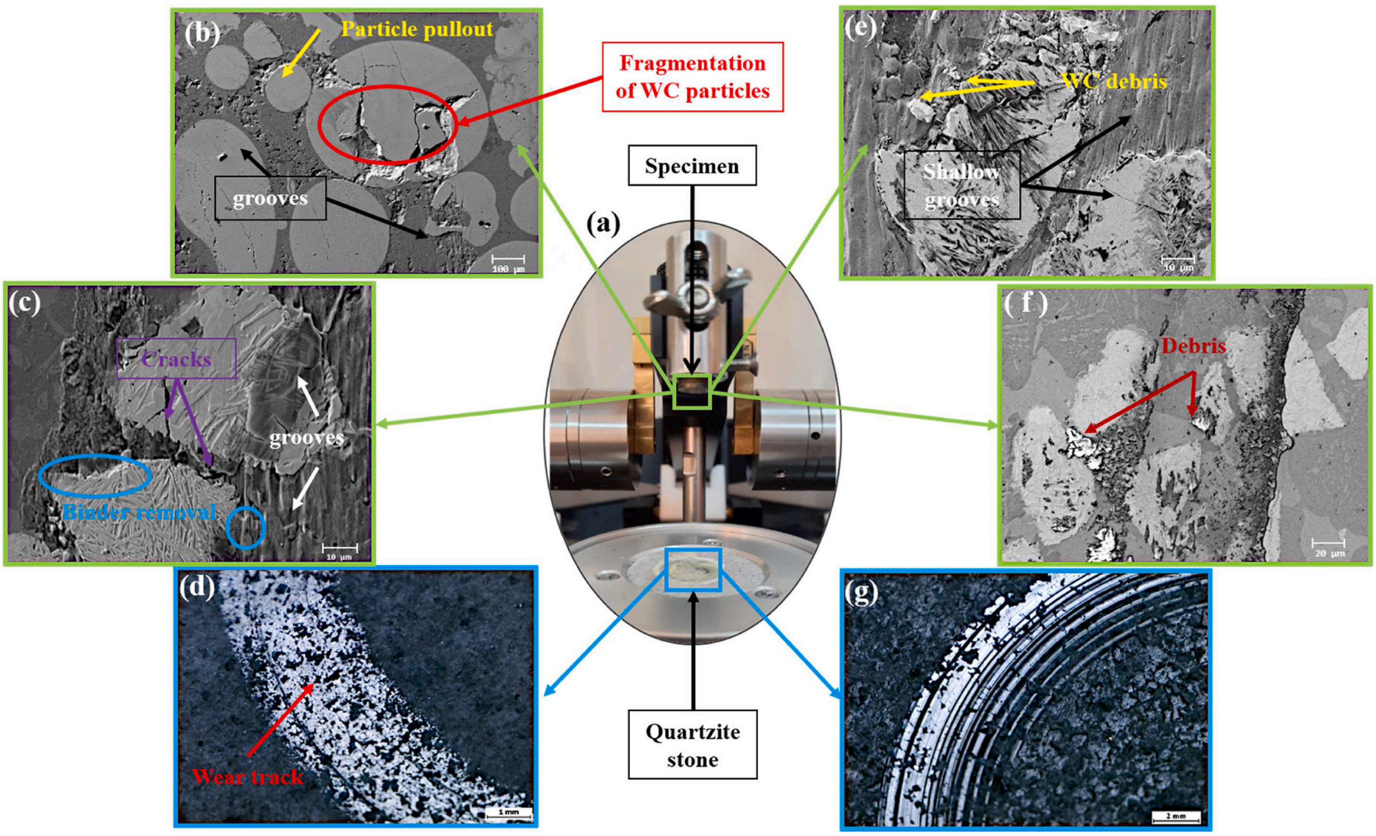

Fig. 14. Worn surfaces (a): specimen emplacement during wear experiment, (b and c): SEM images of the worn surfaces of TIG hard-faced and as-infiltrated specimens under dry conditions, respectively. (e and f): worn surfaces issued from fuel conditions, (d): quartzite counterpart under dry condition and (g): under fuel condition.

conditions, indicating that in dry conditions the abrasion was more severe [16]. Thus, the friction process of wet environment (water and fuel) was more stable and less aggressive than that of dry condition, except for the TIG hard-faced coating in water sliding where high CoF was recorded. The CoF results were confirmed by the wear loss measurements shown in Fig. 13d and Table 4. Both samples exhibited similar behaviour in dry conditions with relatively similar wear loss ranges of samples and stone counterparts (0.8 mg and 0.6 mg for as-infiltrated and TIG hard-faced coating and 14.8 and 15.06 mg for their respective quartzite stones). The lowest wear loss for both samples was obtained in the fuel oil environment while the highest wear loss of the quartzite stone was obtained in the water environment. The increased wear loss of as-infiltrated and TIG hard-faced coating in dry conditions followed their steady-state CoF values. Usually, the harder the material, the lower the wear loss, which improved wear resistance by preventing plastic deformation caused by adhesion [47–49]. Wet conditions sliding gave reduced wear loss of all samples except the TIG hard-faced coating in water sliding, which had high wear damage for the counterpart stone. Based on the wear loss results from Table 4, it is observed that, under fuel conditions, the as-infiltrated sample displays the highest ratio of sample/stone wear loss. Simultaneously, the TIG hard-faced coating under dry sliding reveals the highest one. This suggests substantial wear damage to the quartzite with minimal MMC wear loss in both scenarios.

Analysis of the worn surfaces from different sliding conditions (Fig. 14a) was done using SEM and AFM. Figs. 14b and c shows the abrasive aspect of both samples with shallow grooves on WC particles. The dominant wear mode for as-infiltrated and TIG hard-faced samples in dry conditions was individual WC particles pullout (see AFM images in Fig. 18a and b). This mechanism occurred by fracture and the fragmentation of the hard WC particles in the TIG hard-faced coating (Fig. 14b), which caused the abrasion of the contact surfaces before being lost in the sliding test. Fig. 14b shows small cracks within WC particle/NiCr matrix interface followed by plastic deformation and the removal of material. However, in the as-infiltrated sample, the binder removal around the irregular WC particles was responsible for the particles' pullout as shown in Fig. 14c. This difference in wear behavior was related to the weak cohesion of WC particles with the Cu–Sn matrix and the small pores present in the as-infiltrated samples (Section 3.1), which decreased its wear performance in such harsh conditions. Furthermore, since the metallic matrix of the TIG hard-faced coating was much harder than the as-infiltrated composite, the WC particles protrusion and pull out were more accentuated in the latter (Fig. 18c). Consequently, an

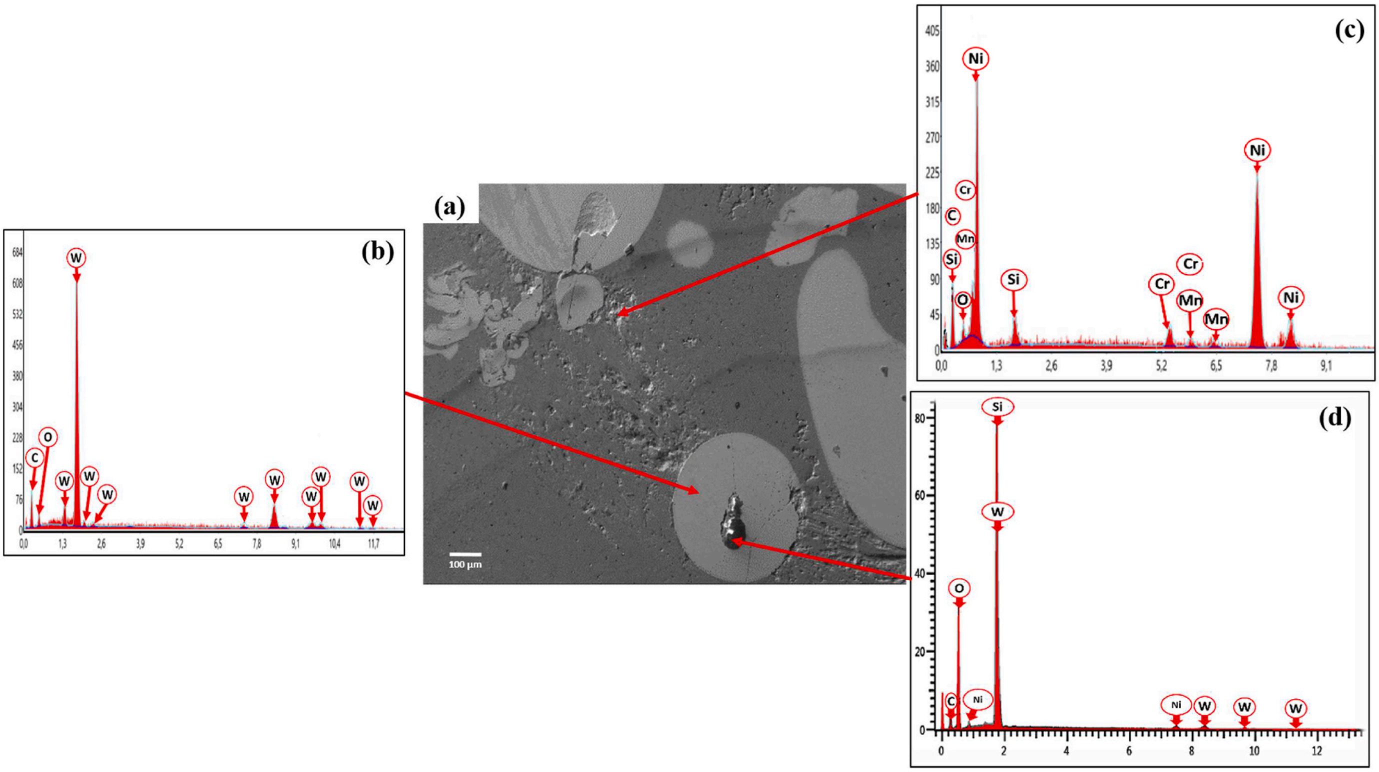

Fig. 15. (a): SEM images of the worn surface of TIG hard-faced specimen under water conditions (b), (c) and (d): EDS point analysis performed on different areas of the worn surface.

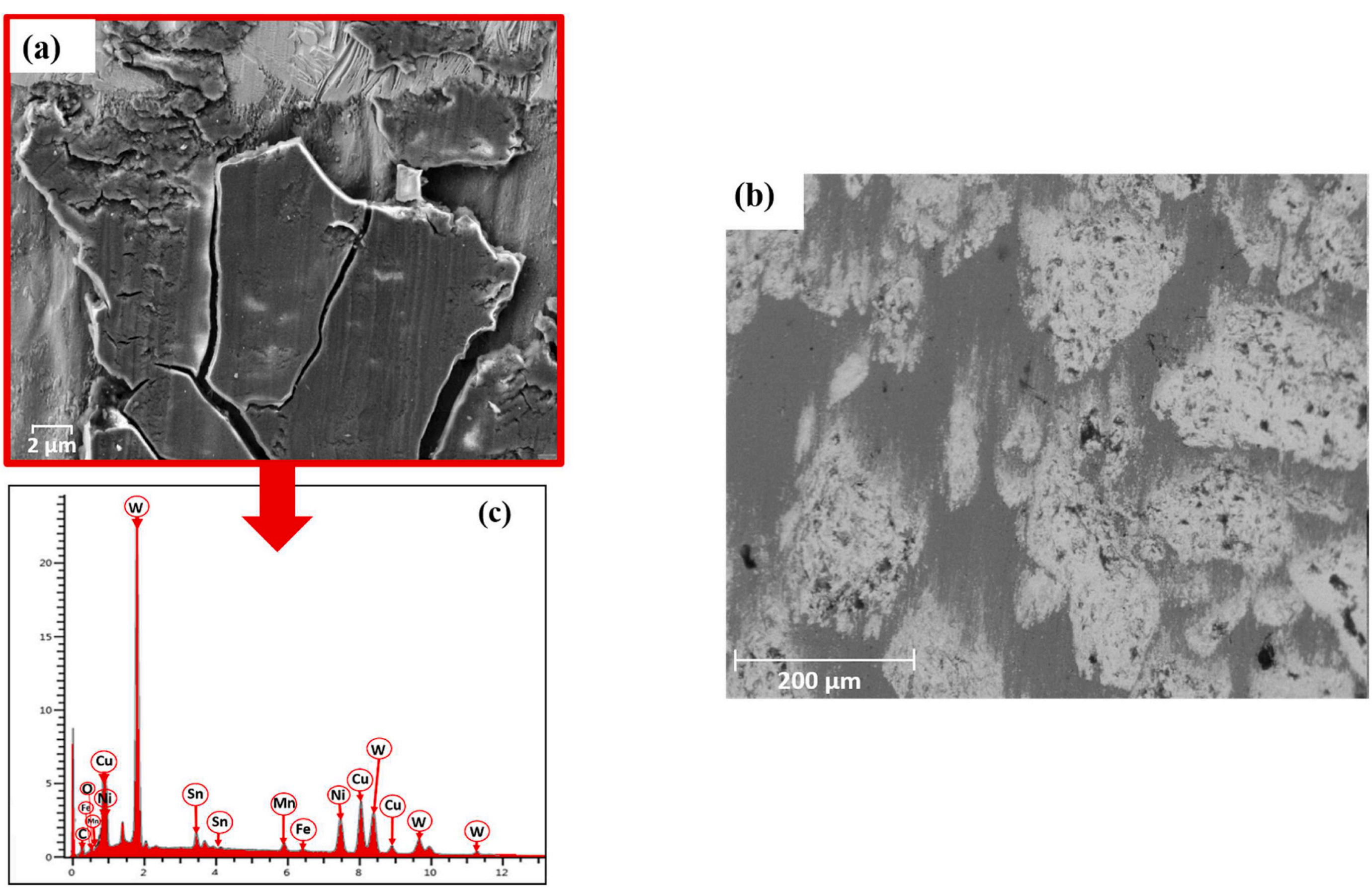

Fig. 16. Worn surface of as-infiltrated specimen under water conditions (a): worn metallic matrix, (b): worn WC particles and (c): EDS analysis of the worn surface.

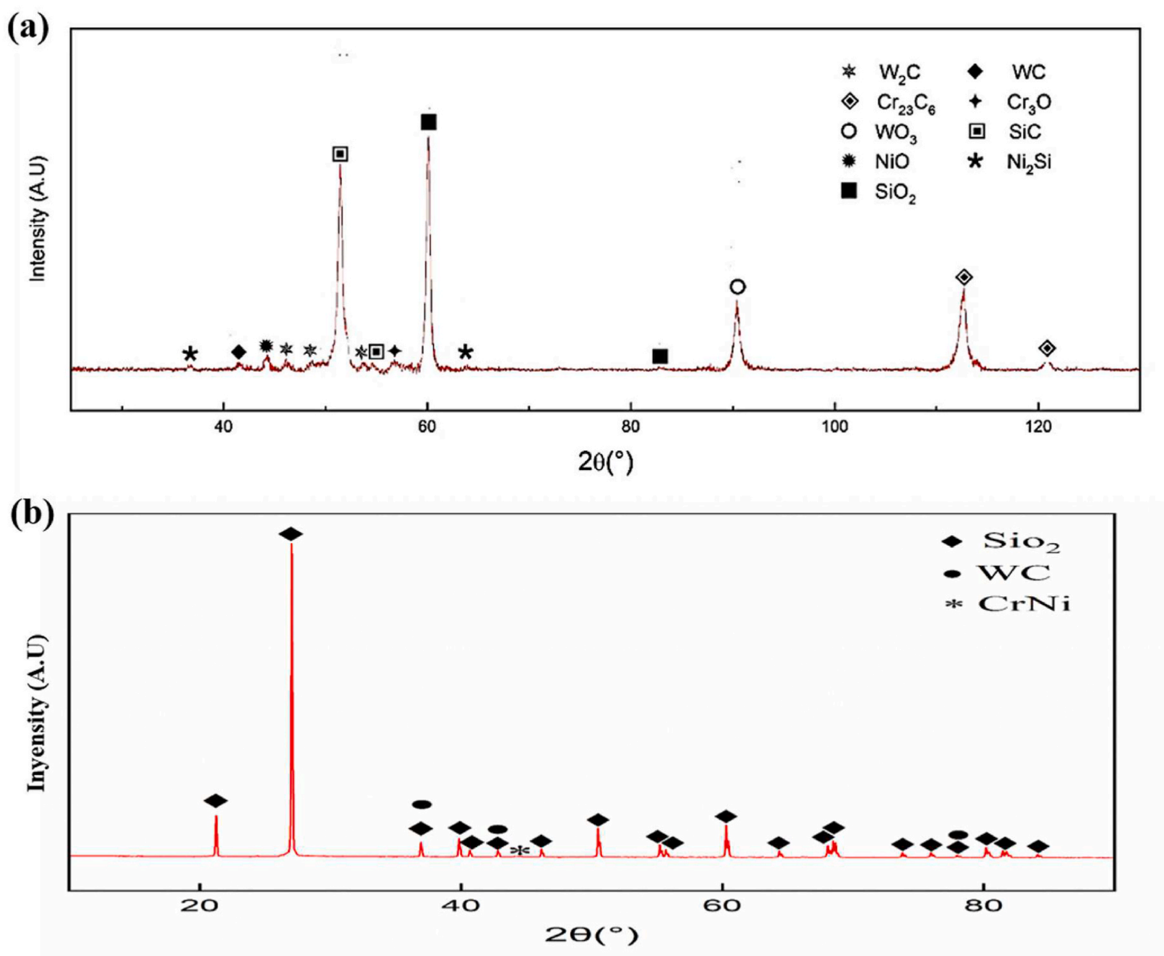

Fig. 17. XRD pattern conducted on the worn surface of the (a): TIG hard-faced coating under water condition and (b): quartzite counterpart under dry conditions.

important amount of WC particles and soft matrix was damaged in the as-infiltrated sample. Conversely, the increased hardness of the NiCr matrix in the TIG-hard-faced coating by the formation of W_2C and $Cr_{23}C_6$ carbides (already observed in the XRD spectrum in Fig. 8b) improved its wear resistance [50]. Simultaneously, the optical micrographs (Fig. 14d and g) of their counterparts wear tracks exhibited similar aspects with grooves on the quartzite surface that were due to abrasion from the WC particles fragmented and detached from all samples. This statement is in good agreement with the XRD point analysis (see Fig. 17b) conducted of the counterpart wear track that revealed the presence of WC phase and NiCr trapped during sliding. By comparison, the wear tracks of the as-infiltrated and TIG hard-faced specimens tested in the fuel condition were much shallower and smoother with the wear scar widths shown in Fig. 14e and f. Wear debris was also trapped between the contact surfaces during sliding. The debris can form a lubricant film that played an abrasive medium and helped to decrease the wear loss and the CoF by the decrease of contact area between the counterpart and the samples [36]. This indicated the prevention of harmful contact between the tested specimens and the quartzite counterparts (Fig. 14g) and decreased the adhesive effect, which agreed with the CoF analyses obtained during sliding wear tests.

When sliding in the TIG hard-faced coating under water, oxidative wear was the main wear mechanism shown by the oxides within the wear track indicated by the dark regions in Fig. 15a. To confirm the dominant wear mechanism in the TIG hardfaced coating, EDS point analysis performed on worn WC particle (Fig. 15b), metallic matrix (Fig. 15c) and on the debris stacked on the wear track surface (Fig. 15d), showed Si which could only have come from the quartzite counterpart indicating adhesive wear. Similar results were found on the wear track of the as-infiltrated water sliding sample shown in Fig. 16a-c. Micro-flacking with delamination of the binder matrix is clearly observed in Fig. 16a. This results in the separation of the WC particles from the Cu–Sn–Ni matrix, which can be gradually worn away through friction (Fig. 16b. The EDS analysis (Fig. 16c) revealed that is mainly composed of Cu, Sn and a small amount of Ni and W elements. This indicates that the surface of the coating undergoes oxidation during the wear process, leading to the formation of oxide products, which is in agreement with Wang et al. [51]. The XRD point analysis conducted on the wear track of the TIG hard-faced sample provided compelling evidence of the oxidative wear mechanism of the coating. This analysis revealed the presence of WO3 oxide, substantiating the oxidation occurring during the wear process. Additionally, SiO2 oxides were detected, which could either have been formed or detached from the quartzite stone during the sliding test, as depicted in Fig. 17a. Notably, on the quartzite worn surface under dry condition, XRD spectrum (Fig. 17b) showed the presence of WC and Ni phases, suggesting a potential abrasion of the TIG-coated sample.

In summary, in dry conditions, abrasive and individual WC particle pullout were the dominant wear mechanisms in the as-infiltrated and TIG hard-faced samples. These mechanisms changed to abrasive in the fuel environment with the presence of debris that played a lubricant film decreasing the wear loss and the surface damage. Conversely, a combination of oxidative and adhesive wear mechanisms was experienced by the TIG hard-faced sample, and the wear damage was more severe on their respective counterparts.

3D AFM images of the worn surfaces of both samples from different

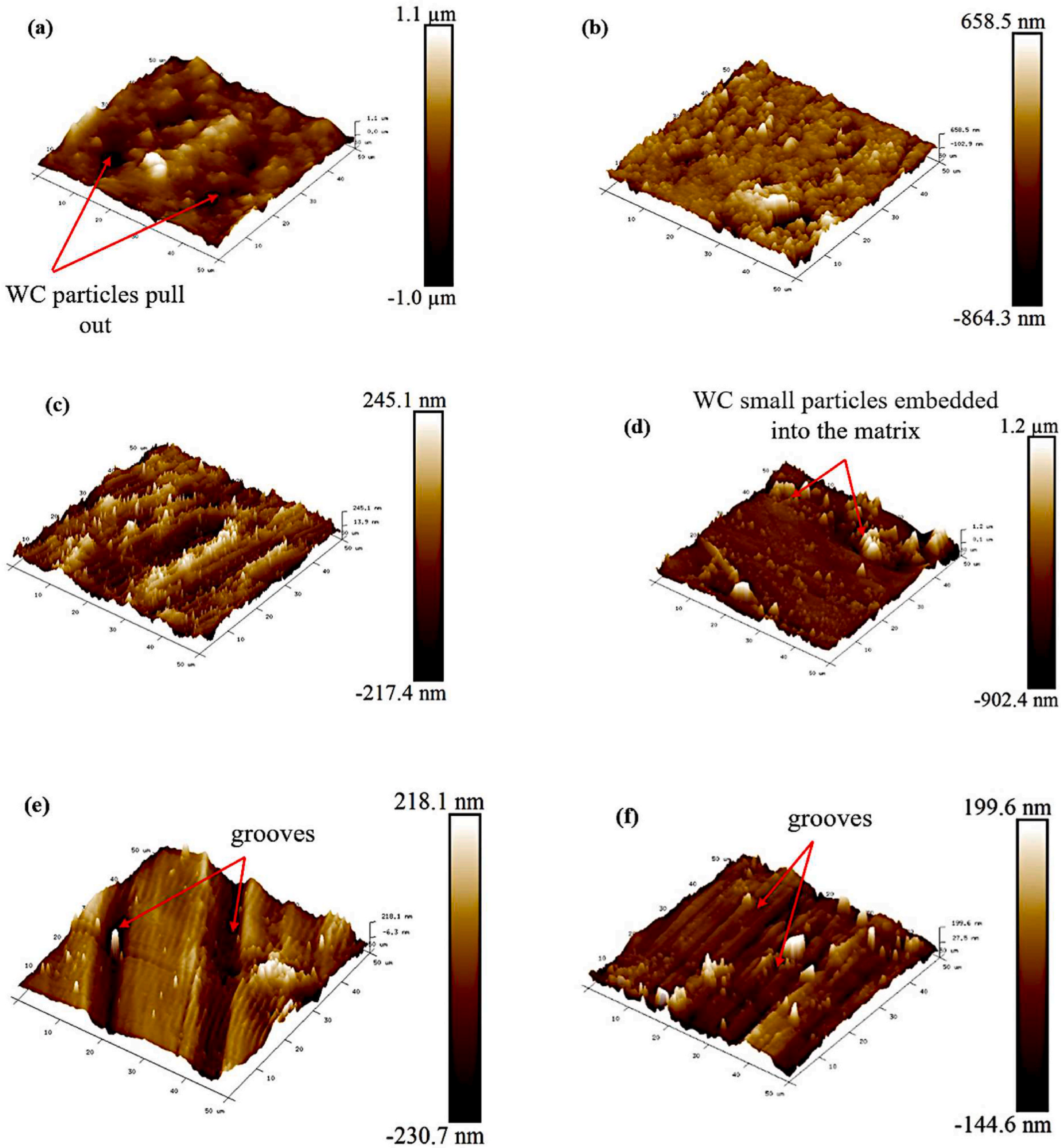

Fig. 18. 3D AFM topography of selected worn surfaces from: dry conditions: (a):as-infiltrated and (b): TIG hard-faced sample, under water condition: (c): as-infiltrated and (d): TIG hard-faced sample and under fuel oil condition: (e): as-infiltrated and (f): TIG hard-faced sample.

Table 5
Roughness measurements on the samples surfaces.

	As infiltrated (nm)	TIG hardfacing (nm)
Dry sliding	615	530
Water sliding	190	241
Fuel sliding	120	131

wear conditions are shown in Fig. 18a-f. The as-infiltrated sample in the dry condition exhibited a rough worn surface (Fig. 18a and b) with roughness Ra = 615 nm followed by the TIG hard-faced coating as shown in Table 5. The surface damage with the WC particles pullout was clearly observed in Fig. 18a. The TIG hard-faced coating subjected to water sliding shown in Fig. 18d had severe wear as characterized by a high amount of the metallic matrix removed with WC particles standing pound during the sliding test. TIG hard-faced coating exhibited shallow grooves under fuel environment with lower roughness, which reflected the mild aspect that underwent the coating during sliding (Fig. 18e–f). Despite the severe wear surface damage under water conditions, the TIG hard-faced coating showed high efficiency with respect to the quartzite stone materials removal.

4. Conclusion

In the present study, an innovative solution for the recovery of worn drilling tools has been presented for the first time. This was demonstrated in the example of a damaged WC-based metal matrix composite (MMC) that was successfully recovered using a WC-Ni/Cr Tungsten Inert Gas (TIG) hardfacing technology. The analysis of the microstructure, hardness and tribological properties of both the as-infiltrated and recovered samples led to the following conclusions:

- The total dissolution of Ni powder into the Cu–Sn binder led to the enhancement of densification of the composite, whereas long infiltration time allowed the formation of secondary carbide (NI_2W_4C) that may have contributed to increasing the hardness of the MMC matrix.
- The interaction between the composite and the TIG hardfacing elements due to diffusion across the interface (Cr and Cu) improved both the adhesion and mechanical properties of the TIG hard-faced sample.
- There was a significant increase in hardness of the TIG hard-faced coating due to the high dissolution and decarburization of WC particles into the NiCr metallic matrix through the formation of $Cr_{23}C_6$ and W_2C carbide phases that hardened the microstructure.
- The TIG hard-faced coating showed high wear performance under dry conditions compared to the as-infiltrated specimen and comparable efficiency under other different conditions.
- The approach outlined in this study regarding the repair of damaged MMC drilling tools, using the TIG hardfacing process, requires further exploration, considering the highly challenging conditions to which the drilling tools in service are subjected.

CRediT authorship contribution statement

Malek Hebib: Conceptualization, Data curation, Formal analysis, Investigation, Writing – original draft. **Lilia Choukrane:** Supervision, Validation, Visualization, Project administration. **Billel Cheniti:** Conceptualization, Formal analysis, Investigation, Methodology, Project administration, Writing – original draft, Writing – review & editing. **Lotfi Faghi:** Supervision, Validation, Visualization. **Alexandra Kovalčíková:** Formal analysis, Investigation, Visualization. **Hamida Bouchafaa:** Resources, Software. **Bouzid Maamache:** Data curation, Resources, Software. **Tamás Csanádi:** Investigation, Methodology, Validation, Visualization, Writing – review & editing. **Pavol Hvizdoš:** Supervision, Validation, Writing – review & editing.

Declaration of competing interest

The authors declare that they have no known competing financial interests or personal relationships that could have appeared to influence the work reported in this paper.

Data availability

No data was used for the research described in the article.

References

[1] C. Hanyaloglu, B. Aksakal, J.D. Bolton, Production and indentation analysis of WC/Fe-Mn as an alternative to cobalt-bonded hardmetals, Mater. Char. 47 (2001) 315–322, https://doi.org/10.1016/S1044-5803(02)00181-X.

[2] B. Cheniti, D. Miroud, P. Hvizdoš, J. Balko, R. Sedlák, T. Csanádi, B. Belkessa, M. Fides, Investigation of WC decarburization effect on the microstructure and wear behavior of WC-Ni hardfacing under dry and alkaline wet conditions, Mater. Chem. Phys. 208 (2018) 237–247, https://doi.org/10.1016/j.matchemphys.2018.01.052.

[3] Z. Guo, J. Xiong, M. Yang, X. Song, C. Jiang, Effect of Mo2C on the microstructure and properties of WC-TiC-Ni cemented carbide, Int. J. Refract. Metals Hard Mater. 26 (2008) 601–605, https://doi.org/10.1016/j.ijrmhm.2008.01.007.

[4] P.Q. Xu, Dissimilar welding of WC–Co cemented carbide to $Ni_{42}Fe_{50.9}C_{0.6}Mn_{3.5}Nb_3$ invar alloy by laser–tungsten inert gas hybrid welding, Mater. Des. 32 (2011) 229–237, https://doi.org/10.1016/j.matdes.2010.06.006.

[5] H. Bouchafaa, D. Miroud, S. Mato, Z. Boutaghou, B. Cheniti, F.J. Pérez, G. Alcalá, Comparative investigation of the Ni and the Fe e ff ect on the structure and mechanical response of a WC-W-Ni hardmetal obtained by infiltration, Int. J. Refract. Metals Hard Mater. 79 (2019) 23–30, https://doi.org/10.1016/j.ijrmhm.2018.11.002.

[6] D. Miroud, M. Tata, s. Lebaili, Consolidation of WC-Ni/W-Ni Double layer composite by infiltration of Cu-Sn-Ni-Mn as binder in SILP process, Asian Journal of Scientific Research 1 (2008) 22–31, https://doi.org/10.3923/ajsr.2008.22.31.

[7] M. Tata, D. Miroud, s. Lebaili, T. Cutard, The study of properties of WC-based and W-based composites fabricated by infiltration with liquid Cu-Mn binder, Asian Journal of Scientific Research 2 (2009) 76–86, https://doi.org/10.3923/ajsr.2009.76.86.

[8] N. Bouzegzi, D. Miroud, F. Ahnia, G. Alcala, S.J. Francisco, K. Khadidja, T. Malik, S. Mato, Microstructural and electrochemical study of a brazed WC based metal matrix composite obtained by in fi ltration process, Journal of Alloys and CompoundsAlloys and Compounds 759 (2018) 22–31, https://doi.org/10.1016/j.jallcom.2018.05.141.

[9] B. Cheniti, D. Miroud, R. Badji, D. Allou, T. Csanádi, M. Fides, P. Hvizdoš, Effect of brazing current on microstructure and mechanical behavior of WC-Co/AISI 1020 steel TIG brazed joint, Int. J. Refract. Metals Hard Mater. 64 (2017), https://doi.org/10.1016/j.ijrmhm.2016.11.004.

[10] P.K. Deshpande, J.H. Li, R.Y. Lin, Infrared processed Cu composites reinforced with WC particles, Mater. Sci. Eng. 429 (2006) 58–65, https://doi.org/10.1016/j.msea.2006.04.124.

[11] A.R. Kennedy, J.D. Wood, B.M. Weager, Wetting and spontaneous infiltration of ceramics by molten copper, J. Mater. Sci. 35 (2000) 2909–2912, https://doi.org/10.1023/A:1004714407371.

[12] I. Daoud, D. Miroud, R. Yamanoglu, Microstructure characterization and quantitative analysis of copper alloy matrix composites reinforced with WC-xNi powders prepared by spontaneous infiltration, Journal of Mining and Metallurgy, Section B 45 (2018) 169–177, https://doi.org/10.2298/JMMB171225005D.

[13] K. Deenadayalan, V. Murali, A. Elayaperumal, A. Satheesh kumar, S. Arulvel, M. Shahedi Asl, Friction and wear properties of short time heat-treated and laser surface re-melted NiCr-WC composite coatings at various dry sliding conditions, J. Mater. Res. Technol. 17 (2022) 3080–3104, https://doi.org/10.1016/j.jmrt.2022.01.124.

[14] S. Liu, H. Wu, S. Xie, M.P. Planche, D. Rivolet, M. Moliere, H. Liao, Novel liquid Ruel HVOF torches fueled with ethanol: relationships between in-flight particle characteristics and properties of WC-10Co-4Cr coatings, Surf. Coating. Technol. 408 (2021) 126805, https://doi.org/10.1016/j.surfcoat.2020.126805.

[15] T. Perrin, S. Achache, P.J. Meausoone, F. Sanchette, Characterization of WC-doped NiCrBSi coatings deposited by Laser Cladding; effects of particle size and content of WC powder, Surf. Coating. Technol. 425 (2021) 127703, https://doi.org/10.1016/j.surfcoat.2021.127703.

[16] Y. Yuan, H. Wu, M. You, Z. Li, Y. Zhang, Improving wear resistance and friction stability of FeNi matrix coating by in-situ multi-carbide WC-TiC via PTA metallurgical reaction, Surf. Coating. Technol. 378 (2019) 124957, https://doi.org/10.1016/j.surfcoat.2019.124957.

[17] C. Just, E. Badisch, J. Wosik, Influence of welding current on carbide/matrix interface properties in MMCs, J. Mater. Process. Technol. 210 (2010) 408–414, https://doi.org/10.1016/j.jmatprotec.2009.10.001.

[18] M.J. Tobar, C. Álvarez, J.M. Amado, G. Rodríguez, A. Yáñez, Morphology and characterization of laser clad composite NiCrBSi-WC coatings on stainless steel, Surf. Coating. Technol. 200 (2006) 6313–6317, https://doi.org/10.1016/j.surfcoat.2005.11.093.

[19] A. Mazouzi, B. Djerdjare, S. Triaa, A. Rezzoug, B. Cheniti, S.M. Aouadi, Effect of annealing temperature on the microstructure evolution, mechanical and wear behavior of NiCr-WC-Co HVOF-sprayed coatings, J. Mater. Res. 35 (2020) 2798–2807, https://doi.org/10.1557/jmr.2020.237.

[20] P.Z. Wang, J.X. Qu, H.S. Shao, Cemented carbide reinforced nickel-based alloy coating by laser cladding and the wear characteristics, Mater. Des. 17 (1996) 289–296, https://doi.org/10.1016/s0261-3069(97)00025-3.

[21] G. Tosun, Ni–WC coating on AISI 1010 steel using TIG: microstructure and microhardness, Arabian J. Sci. Eng. 39 (2012) 2097–2106, https://doi.org/10.1007/s13369-013-0754-3.

[22] S. Buytoz, M. Ulutan, M.M. Yildirim, Dry sliding wear behavior of TIG welding clad WC composite coatings, Appl. Surf. Sci. 252 (2005) 1313–1323, https://doi.org/10.1016/j.apsusc.2005.02.088.

[23] J. Singh, L. Thakur, S. Angra, Abrasive wear behavior of WC-10Co-4Cr cladding deposited by TIG welding process, Int. J. Refract. Metals Hard Mater. 88 (2020) 105198, https://doi.org/10.1016/j.ijrmhm.2020.105198.

[24] J. Shen, L. Campbell, P. Suri, R.M. German, Quantitative microstructure analysis of tungsten heavy alloys (W-Ni-Cu) during initial stage liquid phase sintering, Int. J. Refract. Metals Hard Mater. 23 (2005) 99–108, https://doi.org/10.1016/j.ijrmhm.2004.10.004.

[25] J. Liu, S. Yang, W. Xia, X. Jiang, C. Gui, Microstructure and wear resistance performance of Cu-Ni-Mn alloy based hardfacing coatings reinforced by WC particles, J. Alloys Compd. 654 (2016) 63–70, https://doi.org/10.1016/j.jallcom.2015.09.130.

[26] N. Lin, Y. Jiang, D.F. Zhang, C.H. Wu, Y.H. He, D.H. Xiao, Effect of Cu, Ni on the property and microstructure of ultrafine WC-10Co alloys by sinter-hipping, Int. J. Refract. Metals Hard Mater. 29 (2011) 509–515, https://doi.org/10.1016/j.ijrmhm.2011.02.012.

[27] G. Mühlbauer, G. Kremser, A. Bock, J. Weidow, W.D. Schubert, Transition of W2C to WC during carburization of tungsten metal powder, Int. J. Refract. Metals Hard Mater. 72 (2018) 141–148, https://doi.org/10.1016/j.ijrmhm.2017.12.018.

[28] T. Zhengji, Study of carburization of coarse tungsten powder, Int. J. Refract. Metals Hard Mater. 6 (1987) 221–226, https://doi.org/10.1007/s13632-013-0078-4.

[29] J. Yuan, Y. Huang, L. Wang, C. Jia, F. Zhang, L. Yang, Effect of the dissolution characteristic of tungsten carbide particles on microstructure and properties of Ni-WC/W2C reinforcement coating manufactured by TIG cladding, Int. J. Refract. Metals Hard Mater. 110 (2023) 106047, https://doi.org/10.1016/j.ijrmhm.2022.106047.

[30] Y. Wang, Y. Huang, L. Yang, T. Sun, Microstructure and property of tungsten carbide particulate reinforced wear resistant coating by TIG cladding, Int. J. Refract. Metals Hard Mater. 100 (2021) 105598, https://doi.org/10.1016/j.ijrmhm.2021.105598.

[31] C. Just, E. Badisch, J. Wosik, Influence of welding current on carbide/matrix interface properties in MMCs, J. Mater. Process. Technol. 210 (2010) 408–414, https://doi.org/10.1016/j.jmatprotec.2009.10.001.

[32] N. Bochvar, L. Rokhlin, Carbon – nickel – tungsten, ternary alloy systems phase diagrams, Crystallographic and Thermodynamic (2010) 249–266, https://doi.org/10.1007/978-3-642-02700-0_38.

[33] W. Liu, D. Gao, Microstructure and wear of Ni-WC hardfacing used for steel-body PDC bits, Int. J. Refract. Metals Hard Mater. 101 (2021) 105683, https://doi.org/10.1016/j.ijrmhm.2021.105683.

[34] W.B. Lee, B.D. Kwon, S.B. Jung, Effects of Cr3C2 on the microstructure and mechanical properties of the brazed joints between WC-Co and carbon steel, Int. J. Refract. Metals Hard Mater. 24 (2006) 215–221, https://doi.org/10.1016/j.ijrmhm.2005.04.003.

[35] M. Uzkut, N.K. Sinan, B.S. Unl, The determination of element diffusion in connecting SAE 1040/WC material by brazing, J. Mater. Process. Technol. 169 (2005) 409–413, https://doi.org/10.1016/j.jmatprotec.2005.05.001.

[36] T.B. Torgerson, M.D. Harris, S.A. Alidokht, T.W. Scharf, S.M. Aouadi, R. R. Chromik, J.S. Zabinski, A.A. Voevodin, Room and elevated temperature sliding wear behavior of cold sprayed Ni-WC composite coatings, Surf. Coating. Technol. 350 (2018) 136–145, https://doi.org/10.1016/j.surfcoat.2018.05.090.

[37] Y. Zhang, Y. Epshteyn, R.R. Chromik, Dry sliding wear behaviour of cold-sprayed Cu-MoS2 and Cu-MoS2-WC composite coatings: the influence of WC, Tribol. Int. 123 (2018) 296–306, https://doi.org/10.1016/j.triboint.2017.12.015.

[38] M. Rombouts, R. Persoons, E. Geerinckx, R. Kemps, M. Mertens, W. Hendrix, H. Chen, Development and characterization of nickel based tungsten carbide laser cladded coatings, Phys. Procedia 5 (2010) 333–339, https://doi.org/10.1016/j.phpro.2010.08.154.

[39] M. Surender, B. Basu, R. Balasubramaniam, Wear characterization of electrodeposited Ni–WC composite coatings, Tribol. Int. 37 (2004) 743–749, https://doi.org/10.1016/j.triboint.2004.04.003.

[40] S.A. Alidokht, P. Manimunda, P. Vo, S. Yue, R.R. Chromik, Cold spray deposition of a Ni-WC composite coating and its dry sliding wear behavior, Surf. Coating. Technol. 308 (2016) 424–434, https://doi.org/10.1016/j.surfcoat.2016.09.089.

[41] P. Pereira, L.M. Vilhena, J. Sacramento, A.M.R. Senos, L.F. Malheiros, A. Ramalho, Tribological behaviour of different formulations of WC composites, Wear 204415 (2022) 506–507, https://doi.org/10.1016/j.wear.2022.204415.

[42] P.J. Blau, The significance and use of the friction coefficient, Tribol. Int. 34 (2001) 585–591, https://doi.org/10.1016/S0301-679X(01)00050-0.

[43] N. Gurnagul, M.D. Ouchi, N. Dunlop-Jones, D.G. Sparkes, J.T. Wearing, Factors affecting the coefficient of friction of paper, J. Appl. Polym. Sci. 46 (1992) 805–814, https://doi.org/10.1002/app.1992.070460508.

[44] S.J. Askari, G.C. Chen, F. Akhtar, F.X. Lu, Adherent and low friction nano-crystalline diamond film grown on titanium using microwave CVD plasma, Diam. Relat. Mater. 17 (2008) 294–299, https://doi.org/10.1016/j.diamond.2007.12.045.

[45] D. Cano, A. Lousa, J. Esteve, N. Ferrer-Anglada, Low wear and low friction DLC coating with good adhesion to CoCrMo metal substrates, Phys. Status Solidi B 255 (2018) 1800225, https://doi.org/10.1002/pssb.201800225.

[46] C. Zheng, Y. Liu, J. Qin, C. Chen, R. Ji, Wear behavior of HVOF sprayed WC coating under water-in-oil fracturing fluid condition, Tribol. Int. 115 (2017) 28–34, https://doi.org/10.1016/j.triboint.2017.05.002.

[47] S.A. Alidokht, P. Manimunda, P. Vo, S. Yue, R.R. Chromik, Cold spray deposition of a Ni-WC composite coating and its dry sliding wear behavior, Surf. Coating. Technol. 308 (2016) 424–434, https://doi.org/10.1016/j.surfcoat.2016.09.089.

[48] J.S. Xu, X.C. Zhang, F.Z. Xuan, Z.D. Wang, S.T. Tu, Microstructure and sliding wear resistance of laser cladded WC/Ni composite coatings with different contents of WC particle, J. Mater. Eng. Perform. 21 (2012) 1904–1911, https://doi.org/10.1007/s11665-011-0109-8.

[49] S.A. Alidokht, R.R. Chromik, Sliding wear behavior of cold-sprayed Ni-WC composite coatings: influence OF WC content, Wear 477 (2021) 203792, https://doi.org/10.1016/j.wear.2021.203792.

[50] Q. Wang, Y. Zhang, X. Ding, S. Wang, C.S. Ramachandran, Effect of WC grain size and abrasive type on the wear performance of HVOF-Sprayed WC-20Cr3C2-7Ni coatings, Coatings 10 (2020) 1–14, https://doi.org/10.3390/coatings10070660.

[51] Q. Wang, Q. Li, L. Zhang, D.X. Chen, H. Jin, J. Dong Li, J.W. Zhang, C.Y. Ban, Microstructure and properties of Ni-WC gradient composite coating prepared by laser cladding, Ceram. Int. 48 (2022) 7905–7917, https://doi.org/10.1016/j.ceramint.2021.11.338.